Supplemental Materials

1-Identification and functional characterization of FHR-1$_{L290V}$

Clinical synopsis of the aHUS patient carrying FHR-1$_{L290V.}$

The patient is a 60-year-old male who in March 2008 was admitted to the Emergency Room with a stage 5 renal failure (creatinine 9mg/dL, proteinuria 1.2g/24h, microhematuria >100 hem/field) secondary to an atypical haemolytic-uremic syndrome established by the presence of schistocytosis, undetectable haptoglobin, high LDH, negative Coombs test and normal ADAMST13 levels. Thrombotic microangiopathy (TMA) was confirmed by renal biopsy with glomerular and arteriolar involvement. Secondary causes of TMA were excluded. He was treated with plasmapheresis and Rituximab without response and started hemodialysis few days later. In October 2009, he suffered a seizure's episode attributed to an HTA crisis that was treated with Phenytoin. A complement genetic study performed in 2010 was negative.

On April 8, 2011, he received a kidney graft from a cadaveric donor (CIT of 25 hours) without complications. The graft was functioning from day one, with progressive increase in diuresis and decrease in creatinine. He received tacrolimus, mycophenolate mofetil and steroids as immunosuppression. On the seventh day, a decrease in

diuresis, elevation of BP, and stabilization of creatinine at 2.4 mg / dL were detected concomitant with a decrease in hematocrit, 200,000 platelets, haptoglobin decrease from 87 to 6 mg/dL and LDH increase from 400 to 700 mg/dL. A renal biopsy was performed that ruled out acute rejection and illustrated an important glomerular capillary affectation with endothelial edema and intracapillary thrombus, compatible with a diagnosis of TMA. Renal function deterioration progressed and hemodialysis was initiated. After 70 days of evolution, compassionate treatment with Eculizumab (900mg weekly and then 1200mg every 2 weeks) was finally available. The haematological response was adequate with normalization of anemia, platelets, LDH decrease and rise in haptoglobin up to 189mg/dL. Diuresis only reached to 1L/24h and the patient remained on dialysis. In 2016 it was decided to try a new transplant under prophylaxis with Eculizumab based on the recurrence in the previous transplant. The donor was his wife of 58 years, without contraindications for the donation. Prophylaxis with Eculizumab began a week before, the day before and the day after the transplant and it was continued by 900mg Eculizumab weekly until the 5th week and then increased to 1200mg every two weeks. The intervention (CIT 1h 45m; WIT 2m 40s) was uneventful. Renal function recovered immediately. On the 10th day, a LDH increase and haptoglobin decrease were evidenced. The Coombs test was positive because of the presence of antibodies generated during the previous transfusions. Creatinine was 1.8mg/dL and proteinuria 1.2 g/24h. A biopsy was performed that did not reveal evidence of MAT or acute rejection. Staining for C4d was weakly focally positive in peritubular capillaries. The patient was discharged 14 days after admission. A biopsy at the 6th month showed BK nephropathy without evidence of rejection and recurrence of MAT. A comprehensive genetic analysis in this patient using a NGS panel including all complement genes resulted in the identification of a genetic variant in heterozygosis in *CFHR1* that causes the amino acid substitution in exon 6 (c.868T<G, p.leu290val). No other genetic alterations were found in this patient.

Functional characterization FHR-1_{290V}.

To determine whether the novel FHR-1_{290V} mutant found in our patient is pathogenic, we purified this mutant protein to homogeneity from the patient's plasma using a combination of affinity and gel filtration chromatography. We also expressed a recombinant FHR-1_{L290V} protein in the HEK293 free style expression system to eliminate the heterodimers that FHR-1 forms with FHR-2 and FHR-5 (Figure). Recombinant FHR-1_{L290V} was expressed without any tags and was purified from the culture supernatants using the same protocol used for the plasma-derived protein. Plasma-derived and recombinant FHR-1_{L290V} mutant proteins compete in a dose-

dependent and similar way the regulation by FH (Figure 1). These data demonstrate the pathogenicity of the FHR-1_{L290V} mutant protein and validate the use of recombinant FHR-1 proteins in future functional studies.

Figure

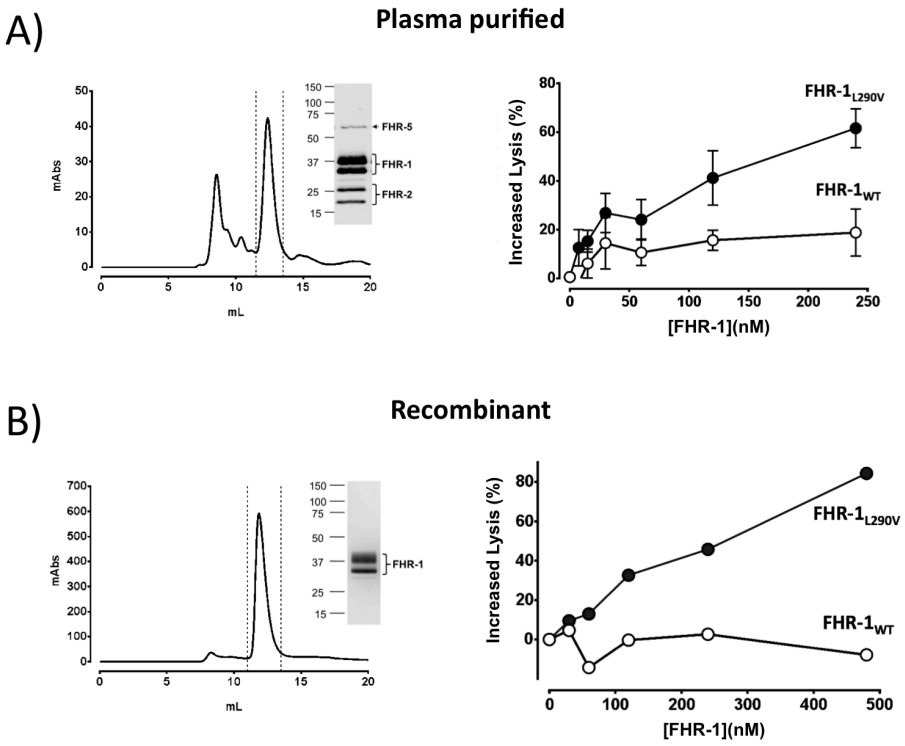

Purification and functional characterization of FHR-1_{L290V} mutant.

A) Left panel shows the gel filtration chromatogram and SDS-PAGE analysis of the FHR-1_{L290V} protein purified from human EDTA plasma and the characterization of its FH de-regulation activity in the sheep hemolysis assay (right panel).

B) Left panel shows the gel filtration chromatogram and SDS-PAGE analysis of the recombinant FHR-1_{L290V} protein purified from HEK293T “free style” cell culture supernatants and characterization of its FH de-regulation activity in the sheep hemolysis assay (right panel).

2-Supplemental Materials and Methods

Genetic analyses.

Genomic DNA was prepared from peripheral blood cells according to standard procedures. Patients were analyzed for mutations in the complement genes using a next generation sequencing (NGS) panels that we developed to screen all the complement genes and some additional genes that have been described relevant to aHUS; 48 genes in total. Targeted genomic capture was performed using Nextera rapid capture custom Enrichment Kit from Illumina and sequencing data generated in a Miseq equipment using Miseq reagent kit v2 (300 cycles). Raw reads were mapped to the human reference genome (UCSC hg19, NCBI build 37.1) (1). Variants were called and annotated against the UCSC hg19 reference genome (2), (3). Common variants with a minor allele frequency value >1% in any population were excluded. Variant annotation was carried out with ANNOVAR. All genetic variants identified were conformed by Sanger in an ABI3730 sequencer using a dye terminator cycle sequencing kit (Applied Biosystems). The analysis of copy number variations within the *CFH-CFHRs* gene region was performed by multiplex ligation-dependent probe amplification (MLPA) with the P236 A1 ARMD mix 1 (MRC-Holland, Amsterdam, Netherlands).

Purification of plasma FHR-1 proteins.

In plasma, FHR-1 presents as a complex set of homo- and hetero-oligomeric molecules with FHR-2 and FHR-5 (4, 5) and it is experimentally not possible to isolate FHR-1 from the other FHR proteins without altering the physiological organization of these complexes. FHR-1_{WT} and mutant FHR-1_{290V} were purified from plasma by immunoaffinity chromatography using our mouse monoclonal antibody 2C6 as previously described (6). Briefly, filtered plasma was loaded into a CNBr-activated sepharose (GE Healthcare) column coupled with mAb 2C6. Bound protein was eluted at low pH, and fractions containing the protein were pooled, concentrated and further purified to homogeneity using a size exclusion column (GE Healthcare), and stored at -80ºC prior to use in 10 mM Hepes, 150 mM NaCl, pH7.4 buffer.

NMR Spectroscopy: Saturation Transfer Difference (STD-NMR).

3'-Sialyllactose (3'-SL) and 6'-Sialyllactose (6'-SL) were purchased from Carbosynth (UK). 1D-1H and 2D TOCSY and HSQC spectra were acquired to assign the signals and confirm the structure of compounds as previously described (7). The STD-NMR spectra were acquired using 3mm tubes (200 µL sample volume) and a Bruker AVIII-600 spectrometer equipped with a room temperature TXI probe head or

TXI crioprobe controlled with TOPSPIN software (Bruker). Samples contained between 0.5 to 1mM of sialylated ligand (3'-SL or 6´-SL) and protein in the range of 10μM±5μM (in an approximate ratio ligand:protein 50:1). Different samples with full length FH; FHR1 and mutants of FH and FHR1 were studied. Protein samples were prepared in buffer 20mM potassium phosphate pH 7.4, 150mM NaCl in D_2O and the sialyl lactose ligands were added up to the required concentration (ligand:protein 50:1) from 40mM stock solutions prepared in D_2O. Different temperatures during spectra acquisition, 278, 288, 298K were tested, spectra obtained at 288K are presented. Standard Bruker sequences for STD-NMR, "stddiff" and "stddiffesgp" were used and the spectra were processed with TOPSPIN 3.5 software. Selective saturation of the protein was achieved by using a train of 60 Gaussian-shaped pulses of 50-ms each, to attain a saturation time of 3s and a total relaxation delay of 4s. The spectra were acquired with 512 scans and 32k points in the direct dimension. The residual HDO signal was suppressed, when needed, by excitation sculpting gradient (*esgp*). Reference experiments of protein alone, in the absence of ligand, were run under the same conditions to identify protein background signals. An off-resonance frequency of δ=100ppm and two on-resonance frequencies of δ=-0.14/7.1ppm were applied for selective saturation of protein resonances, targeting spectrum regions where no signals were observed for sialylated ligands. To exclude non-specific saturation of ligand protons upon irradiation, control STD-NMR experiments of the ligands were performed in the absence of protein.

Protein and ligand preparation for computational studies.

The coordinates of C3d, FH, FHR-1, and FHR-1_{A296V} were obtained from the corresponding X-ray crystallographic structures (PDB IDs: 5NBQ -chain C- for C3d; 2G7I and 4ONT -chain E- for FH; 4MUC -chain A- for FHR-1, and 3RJ3 -chain F- for FHR-1_{A296V}). In the case of FHR-1_{L290V}, we built a model using FHR-1 structure (PDB ID 4MUC) as template, by mutation of residue 290 with PyMOL (8). All structures were prepared with PrepWiz tool included in Maestro (9). Water molecules and co-crystallization factors were removed, missing residues and capping termini were added, and hydrogens were added with PROPKA (10) at physiological pH. The protonation state of histidines was considered as HID for the His60, in FH, FHR-1 and FHR-1_{L290V} and His108 in FH, and as HIE for the His108 in FHR-1, FHR-1_{L290V} and FHR-1_{A296V}, and His60 in FHR-1_{A296V} according to residues nearby. Disulfide bonds were also defined. The final structures of the proteins were minimized with OPLS3 force field.

The 3D structure of 3'SL was extracted from the X-ray crystallographic structure of the complex of FH with C3d (PDB ID 4ONT), and the 3D structure of 6'SL was built with the GLYCAM carbohydrate builder (11). Both structures were optimized with Macromodel (Maestro) (12), with MM3* force field. Charge distribution was also calculated.

Molecular dynamics (MD) simulations.

The studied proteins, the ligands (3'SL and 6'SL), and the corresponding protein-protein and protein-ligand complexes were prepared with tleap module within the AMBER14 suite (13), and solvated with explicit TIP3P water, arranged in a truncated octahedron box 10Å from the surface of the protein. The charges were neutralized upon the addition of Cl^- ions. The force fields used were ff14SB (14) for the proteins and GLYCAM06 for the carbohydrates. The MD simulations were carried out by using the sander and CUDA modules in AMBER14 (13). For all hydrogen-containing bonds, the SHAKE algorithm was applied, using a 2fs integration step. Periodic boundary conditions were applied, and also the particle mesh Ewald method to consider the long-range electrostatic interactions, with a grid spacing of 1.0 Å. The cutoff for non-bonded interactions was set on 9.0 Å. Once the systems were built, energy minimization of the solvated systems was performed by applying harmonic potential restrictions on the protein. First, harmonic potential constraint of 100 kcal mol^{-1} $Å^{-2}$ was applied to the solute during 1000 steps of steepest descent algorithm, followed by 7000 steps of conjugate gradient algorithm. After that, the harmonic potential restraints were gradually reducing to 10, 5 and 1.5 kcal mol^{-1} $Å^{-2}$ every 600 steps until no restraints were applied. Then the systems were heated from 0 to 100K using the Langevin thermostat applying a 20 kcal mol^{-1} $Å^{-2}$ harmonic potential restraint for the solute, in the canonical ensemble. The system was then heated from 100K to 300K, with restraint of 20 kcal mol^{-1} $Å^{-2}$, in the isothermal-isobaric ensemble and, finally, an unrestrained simulation of 100ps was performed. After that, the production phase was run at 300K for 500ns using the Langevin thermostat with a collision frequency of 1.0 ps^{-1}, under isothermal-isobaric conditions. The analysis of the trajectories was performed with the cpptraj module included in the AMBER14 software package, and visualized with VMD (15).

Molecular Electrostatic Potential Surfaces.

The molecular surfaces were calculated with Maestro, with a probe radius of 1.4Å, a VDW radius scale of 1.0Å, and high surface resolution. The electrostatic

potential surface was displayed with a color ramp from red to blue, with a maximum and a minimum of -0.3 and +0.3 respectively.

Protein-protein docking studies.

The docking was performed by using the ClusPro server (16). The following resides were set-up as interacting residues: K1105, I1108, L1109, K1111, K1113, P1114, D1115, G1116, E1160, Q1161, N1163, S116,4 and K1171 for C3dg; and residues D218, I219, S221, F222, P223, Q236, Q238, N239, Y241, K287, and Y289 for FHR-1, FHR-1_{L290V} and FHR-1_{A296V}. The refined structure of C3d was docked towards six different structures corresponding to four proteins: FH (refined X-ray structure), FHR-1 (refined X-ray structure and one structure from the MD simulation), FHR-1_{A296V} (one conformation from the MD simulation), FHR-1_{L290V} (two conformations from the MD simulation). FH was included to validate the docking protocol. The results obtained shown docked C3d/FH poses according to the X-ray crystallographic pose in PDB ID 4ONT. The selected conformations of FHR-1, FHR-1_{A296V}, and FHR-1_{L290V} were extracted from the MD simulations: one from the major cluster (for FHR-1, and FHR-1_{A296V}), and two from the two major clusters (for FHR-1_{L290V}).

3'SL and 6'SL docking studies.

Two different docking programs, Glide (17) and AutoDock (18), were used to run the docking calculations of ligands 3'SL and 6'SL. As receptors, nine different structures corresponding to four proteins were considered: FH (two refined X-ray structures from PDB 4ONT -chain E-, and PDB 2G7I, and one conformation from the MD simulation of PDB 2G7I), FHR-1 (refined X-ray structure from PDB 4MUC -chain A-, and one conformation from the MD simulation), FHR-1_{A296V} (refined X-ray structure from PDB 3RJ3 -chain F-, and one conformation from the MD simulation), FHR-1_{L290V} (two conformations from the MD simulation). The selected conformations of FH, FHR-1, FHR-1_{A296V}, and FHR-1_{L290V} were extracted from the major clusters from the MD simulations. In all cases, the receptor grid was centered at the sialic acid binding site. For Glide, the grid size was set to dock ligands with a length =< than 20Å and the inner box size was set to 12x12x12Å. The XP mode was run with the default settings, with no constraints, and generating 50 poses per ligand. In the case of AutoDock, the grid size was 40x40x40 points, and the grid spacing was 0.375Å. The Lamarckian Genetic Algorithm was used, and the default parameters were chosen except for the GA runs that were set to 200. Validation of the docking protocol was performed by using 3'-SL and FH. The predicted docked poses in FH were in agreement with the X-ray crystallographic pose (PDB ID 4ONT).

References

1 Langmead B, Salzberg SL. Fast gapped-read alignment with Bowtie 2. *Nat Methods*. 2012;9(4):357-9.

2. Koboldt DC, Zhang Q, Larson DE, et al. VarScan 2: somatic mutation and copy number alteration discovery in cancer by exome sequencing. *Genome Res*. 2012;22(3):568-76.

3. Wang K, Li M, Hakonarson H. ANNOVAR: functional annotation of genetic variants from high-throughput sequencing data. *Nucleic Acids Res*. 2010;38(16):e164.

4. Goicoechea de Jorge E, Caesar JJ, Malik TH, et al. Dimerization of complement factor H-related proteins modulates complement activation in vivo. *Proceedings of the National Academy of Sciences of the United States of America*. 2013;110(12):4685-90.

5. Goicoechea de Jorge E, Tortajada A, Garcia SP, et al. Factor H Competitor Generated by Gene Conversion Events Associates with Atypical Hemolytic Uremic Syndrome. *Journal of the American Society of Nephrology : JASN*. 2018;29(1):240-9.

6. Valoti E, Alberti M, Tortajada A, et al. A Novel Atypical Hemolytic Uremic Syndrome - Associated Hybrid CFHR1/CFH Gene Encoding a Fusion Protein That Antagonizes Factor H-dependent Complement Regulation. *J Am Soc Nephrol*. 2015;26(1):209-19.

7. Blaum BS, Hannan JP, Herbert AP, et al. Structural basis for sialic acid-mediated self-recognition by complement factor H. *Nature chemical biology* 2015, 11(1): 77-82.

8. Schrödinger L. The PyMOL Molecular Graphics System, Version 2.0, https://www.schrodinger.com/pymol. 2020.

9. Schrödinger L. Schrödinger Release 2020-2: Maestro, New York, NY, www.schroedinger.com/maestro. 2020.

10. Olsson MH, Søndergaard CR, Rostkowski M, Jensen JH. PROPKA3: Consistent Treatment of Internal and Surface Residues in Empirical pKa Predictions. *Journal of chemical theory and computation*. 2011;7(2):525-537.

11. Group W. GLYCAM Web. Complex Carbohydrate Research Center, University of Georgia, Athens, GA, http://glycam.org. 2005-2020.

12. Schrödinger L. Schrödinger Release 2020-1: MacroModel, Schrödinger, LLC, New York, NY, https://www.schrodinger.com/macromodel. 2020.

13. D.A. Case VB, J.T. Berryman, R.M. Betz, Q. Cai, D.S. Cerutti, T.E. Cheatham, III, T.A. Darden, R.E.Duke, H. Gohlke, A.W. Goetz, S. Gusarov, N. Homeyer, P. Janowski, J. Kaus, I. Kolossváry, A. Kovalenko,T.S. Lee, S. LeGrand, T. Luchko, R. Luo, B. Madej, K.M. Merz, F. Paesani, D.R. Roe, A. Roitberg, C. Sagui,R. Salomon-Ferrer, G. Seabra, C.L. Simmerling, W. Smith, J. Swails, R.C. Walker, J. Wang, R.M. Wolf, X.Wu and P.A. Kollman (2014), AMBER 14, University of California, San Francisco. AMBER 14, University of California, San Francisco, https://ambermd.org. 2014.
14. Maier JA, Martinez C, Kasavajhala K, et al. ff14SB: Improving the Accuracy of Protein Side Chain and Backbone Parameters from ff99SB. *Journal of chemical theory and computation*. 2015;11(8):3696-3713.
15. Humphrey W, Dalke A, Schulten K. VMD: visual molecular dynamics. *Journal of molecular graphics*. 1996;14(1):33-38,27-38.
16. Kozakov D, Hall DR, Xia B, et al. The ClusPro web server for protein-protein docking. *Nature protocols.* 2017;12(2):255-278.
17. Schrödinger L. Schrödinger Release 2020-2: Glide, Schrödinger, LLC, New York, NY, www.schroedinger.com/glide. 2020.
18. Morris GM, Huey R, Lindstrom W, et al. AutoDock4 and AutoDockTools4: Automated docking with selective receptor flexibility. *Journal of computational chemistry.* 2009;30(16):2785-2791.

3- Supplemental Figure 1

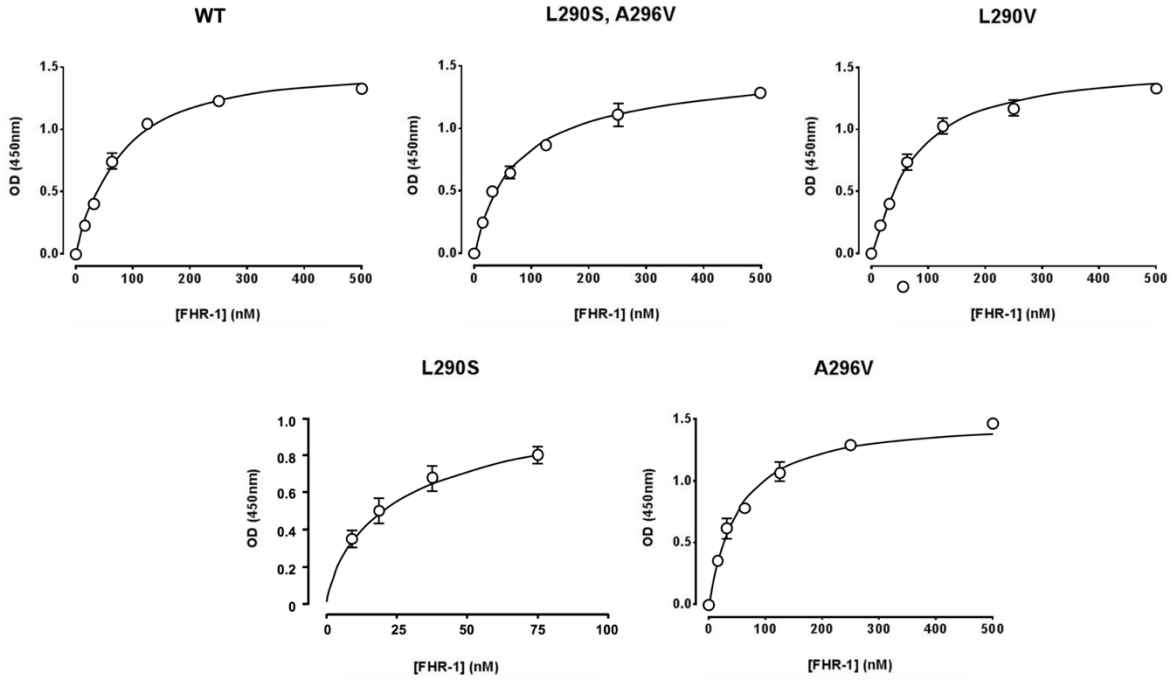

FHR-1$_{WT}$ and the FHR-1 mutants bind to nC3

The different FHR-1 proteins were added at different concentrations to ELISA plates coated with nC3 and incubated for 1h at RT. Bound FHR-1 was detected using a biotynilated 2C6 mAb (anti FHR-1) and followed by HRP-conjugated streptoavidin. After incubation with TBM substrate and 0.1M sulfuric acid to stop the reaction, absorbance was measured at 450nm.

4- Supplemental Figure 2

A)

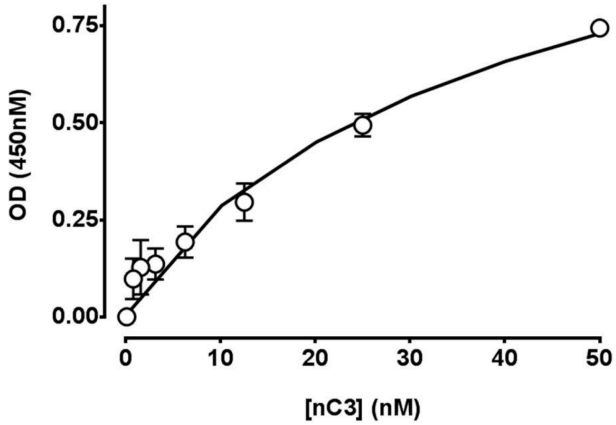

Binding of native C3 to immobilized FHR-1. Different amounts of nC3 were added to ELISA plates coated with FHR-1 and incubated for 1h at RT. Bound C3 was detected using a rabbit anti human C3 antibody and followed by HRP-conjugated goat anti rabbit Igs antibody. After incubation with TBM substrate and 0.1M sulfuric acid to stop the reaction, absorbance was measured at 450nm.

B)

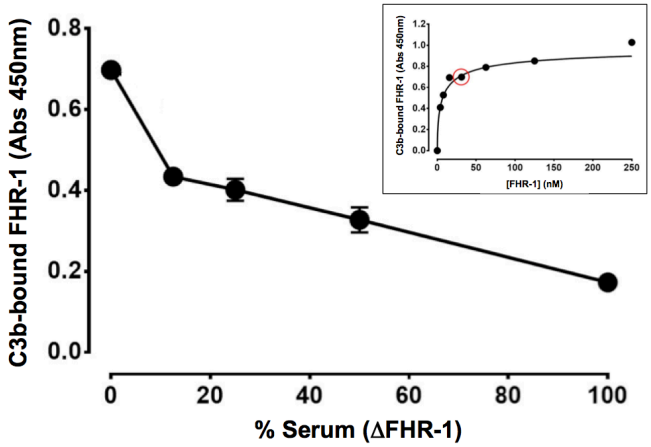

Binding of FHR-1 to immobilized C3b is reduced in the presence of serum. Different amounts of FHR-1 were added to ELISA plates coated with C3b to determine the minimum concentration of FHR-1 that provides maximum binding (inset). Then, this concentration was added to different % of human serum depleted of FHR-1 and added to the C3b coated ELISA plates. Bound FHR-1 was detected using a biotynilated 2C6 mAb (anti FHR-1) and followed by HRP-conjugated streptoavidin. After incubation with TBM substrate and 0.1M sulfuric acid to stop the reaction, absorbance was measured at 450nm.

5- Supplemental Figure 3

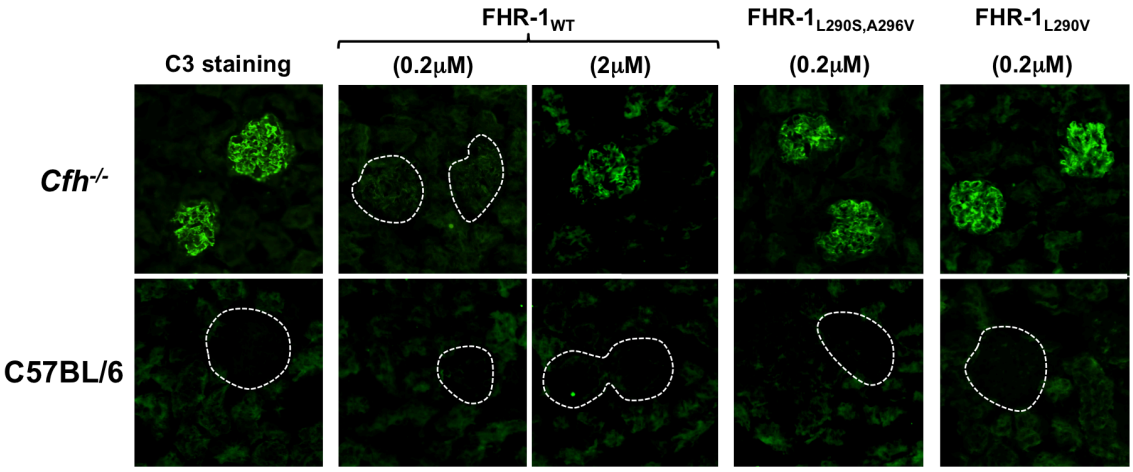

FHR-1_{WT} and aHUS-associated FHR-1 mutants bind only to C3-opsonized glomeruli.

FHR-1_{WT}, FHR-$1_{L290S,A296V}$ and FHR-1_{L290V} were added to *Cfh* $^{-/-}$ and *C57BL/6* cryostat kidney sections. The binding of FHR-1 was detected using the mAb 2C6 (biotinylated). Dotted circles are shown to illustrate the presence of the glomeruli in the absence of FHR-1 binding.

6- Supplemental Figure 4

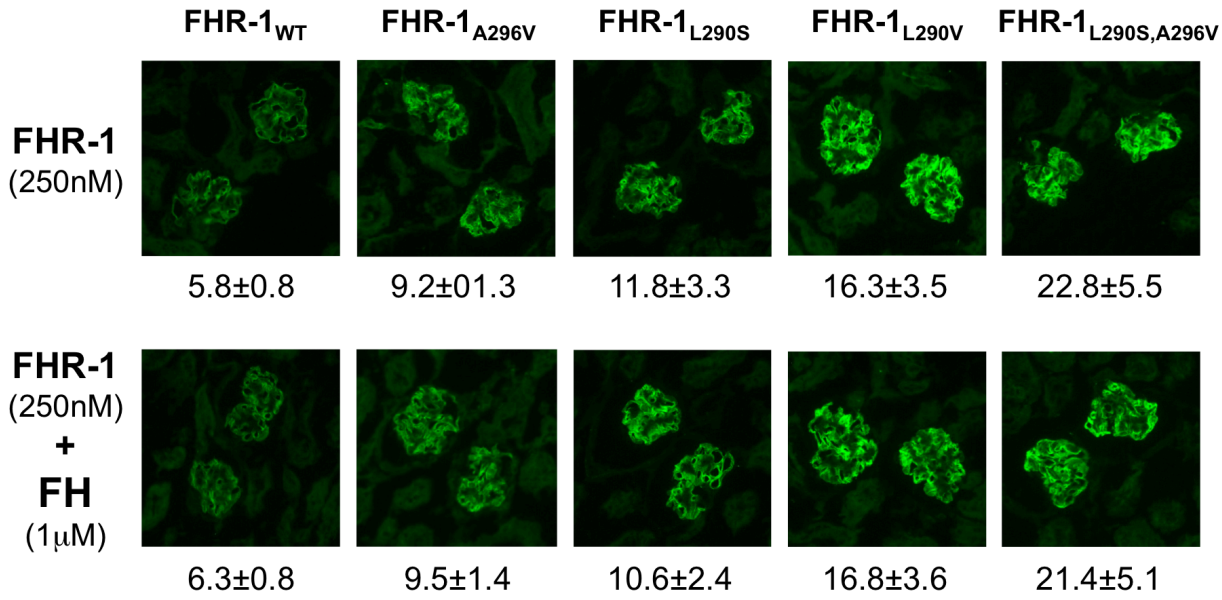

Lack of competition between FH and FHR-1 proteins for binding to *Cfh*$^{-/-}$ glomeruli.

Cryostat kidney sections from *Cfh*$^{-/-}$ mice were incubated with 250nM of the different FHR-1 proteins alone, or with four molar excess of FH. FHR-1 proteins were detected using the mAb 2C6 (biotinylated). Fluorescence intensity (FI) is expressed in arbitrary units (AU). Data are mean ± SD of a minimum of 20 glomeruli.

7- Supplemental Figure 5

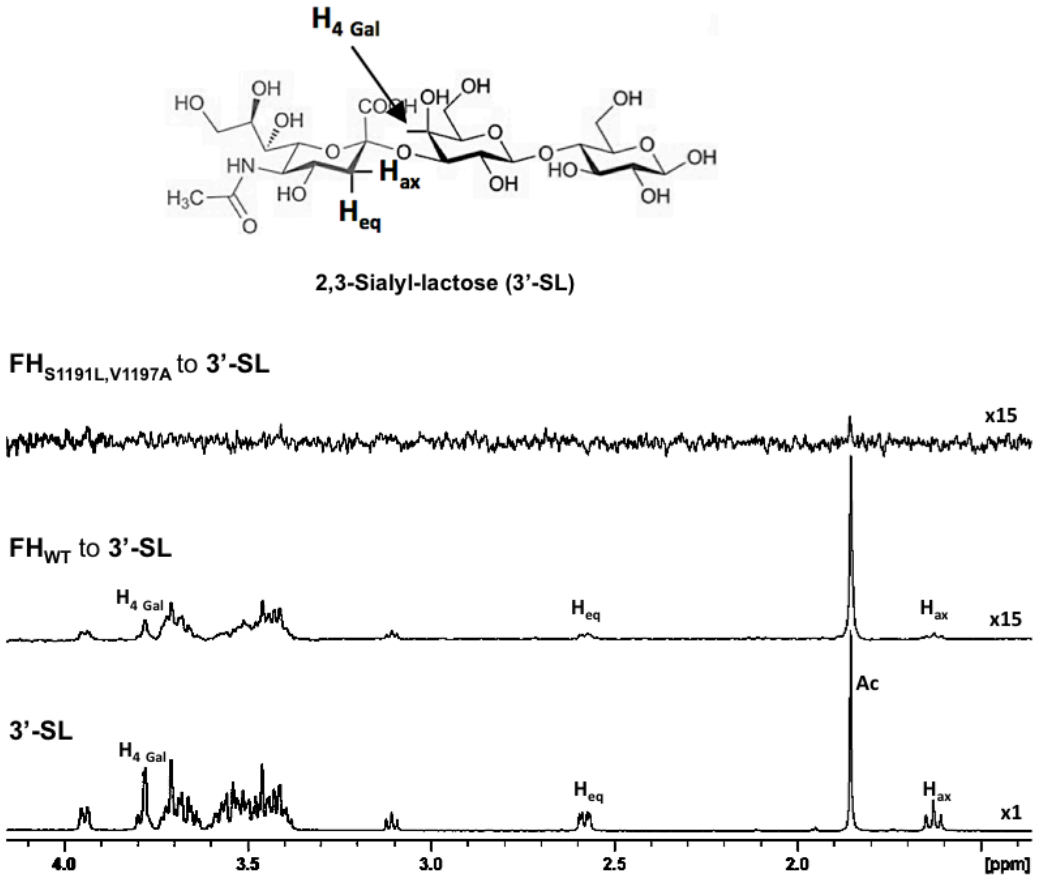

STD: Saturation Transfer Difference spectrum, *off*-protein minus *on*-protein
Selective irradiation on the protein transfer saturation only to protons of bound ligands

Substituting the C-ter of FH with that of FHR-1 eliminates binding to 3'-SL

Saturation transfer difference spectra with 3'SL: lower panel, reference spectra of 3'SL corresponding to the off-resonance spectra acquired in presence of FHR-1_{WT}. Above this are panels showing the STD difference spectra in presence of: FH_{WT} wt and $FH_{S1191L,V1197A}$, the acetate of the 5-NAc group of the sialic residue received the highest saturation. In both cases 3'SL concentration was adjusted to 50:1 ligand protein ratio. Structures of 3'-sialyllactose, 3'SL, (α-Neu5Ac-(2-3)-β-D-Gal-(1-4)-D-Glc) is shown at the top. All STD spectra were acquired with 3s saturation on -0.14ppm. Background signal of protein were subtracted in each case from a spectra of the protein acquired under the same conditions but in absence of ligand. Signals of selected protons are labeled.

8- Supplemental Figure 6

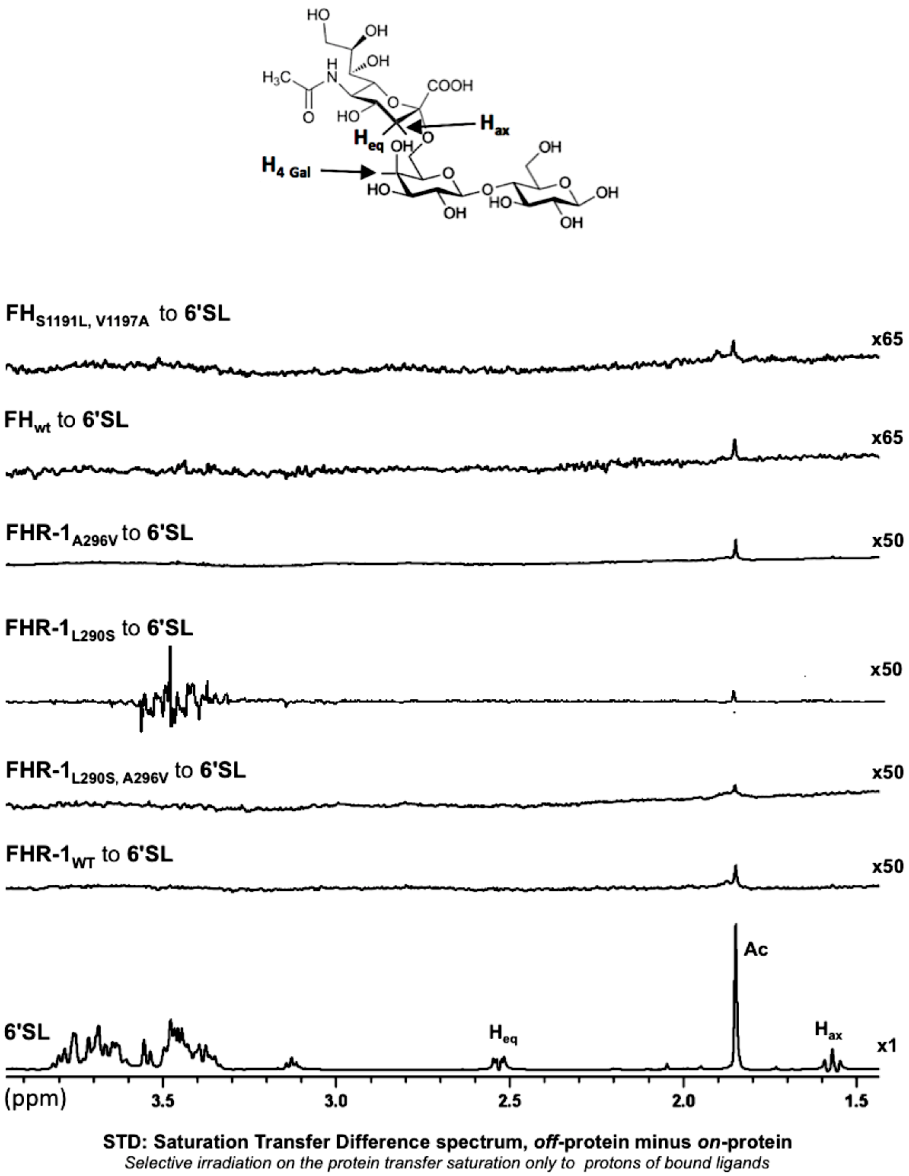

STD: Saturation Transfer Difference spectrum, *off*-protein minus *on*-protein
Selective irradiation on the protein transfer saturation only to protons of bound ligands

FHR-1$_{290V}$ is the only FHR-1 protein that binds 6'-SL

From bottom to top the panels show respectively: Off reference spectra of 6'SL, the STD difference spectra of 6'SL in presence of FHR-1$_{WT}$; FHR-1$_{L290S,A296V}$; FHR-1$_{L290S}$; FHR-1$_{A296V}$; FH$_{WT}$ and FH$_{S1191L,V1197A}$. In all cases the observed saturation of acetate of the 5-NAc group of the sialic residue was below 0.5% corresponding to unspecific saturation in absence of protein. Concentrations were adjusted to 50:1 ligand protein ratio. Structure of 6'-sialyllactose, 6'SL, (α-Neu5Ac-(2-6)-β-D-Gal-(1-4)-D-Glc) is shown at the top. All STD spectra were acquired with 3s saturation on -0.14ppm. Background signal of protein were subtracted in each case from a spectrum of the protein acquired under the same conditions but in absence of ligand. Signals of selected protons are labeled.

9- Supplemental Figure 7

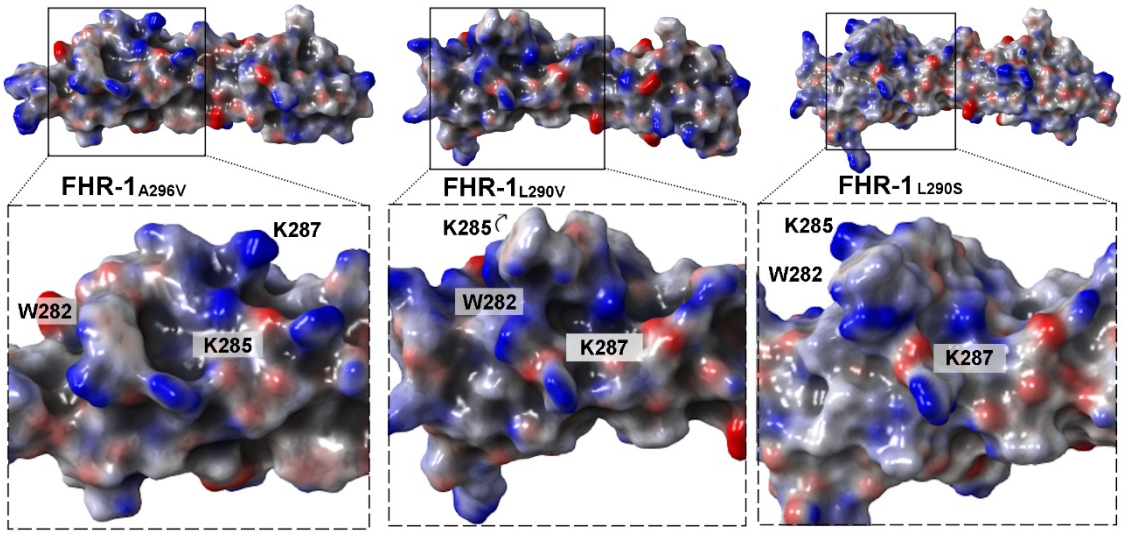

Structure of the sialic binding site in the FHR-1 mutants.

Electrostatic potential surface (EPS) of FHR-1_{A296V} (left), FHR-1_{L290V} (center) and FHR-1_{L290S} (right) from the MD simulations. The sialic acid binding site is highlighted in a square and enlarged below.

10- Supplemental Figure 8

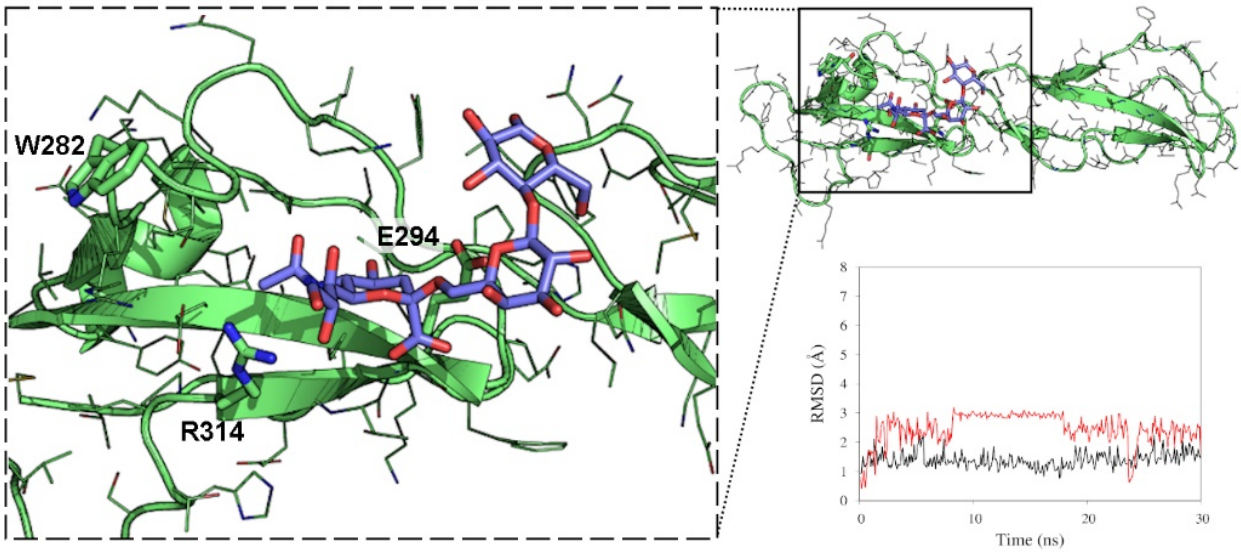

MD simulations of the FHR-1_{L290V}/6'SL complex.

FHR-1_{L290V}/6'SL complex (green/blue) from docking calculations. RMSD (calculated with heavy atoms for the protein and with carbons for the 6'SL) from the MD simulation is also depicted (complex in black, 6'SL in red).